Thermomigration induced microstructure and property changes in Sn-58Bi solders

Shen, Yu-An; Zhou, Shiqi; Li, Jiahui; Tu, K.N.; Nishikawa, Hiroshi

Published in:
Materials and Design

Published: 15/03/2019

Document Version:
Final Published version, also known as Publisher's PDF, Publisher's Final version or Version of Record

Published version (DOI):
10.1016/j.matdes.2019.107619

Publication details:
Shen, Y-A., Zhou, S., Li, J., Tu, K. N., & Nishikawa, H. (2019). Thermomigration induced microstructure and property changes in Sn-58Bi solders. Materials and Design, 166, [107619]. https://doi.org/10.1016/j.matdes.2019.107619

Materials and Design 166 (2019) 107619

Contents lists available at ScienceDirect

Materials and Design

journal homepage: www.elsevier.com/locate/matdes

Thermomigration induced microstructure and property changes in Sn-58Bi solders

Yu-An Shen [a,*], Shiqi Zhou [a,b], Jiahui Li [c], K.N. Tu [d], Hiroshi Nishikawa [a,*]

[a] Jointing and Welding Research Institute (JWRI), Osaka University, Osaka 5600047, Japan
[b] Graduate School of Engineering, Osaka University, Osaka 565-0871, Japan
[c] Department of Electronic Engineering, City University of Hong Kong, Hong Kong, China
[d] Department of Materials Science and Engineering, UCLA, Los Angeles, CA, USA

HIGHLIGHTS

- The thermomigration behavior in Cu/Sn58Bi/Cu joints is hardly seen, not to mention the process and details.
- Bi accumulation at the cold end by thermomigration induces a significant Sn-Bi phase separation in the Sn-58Bi solder joints.
- The growth of Cu-Sn intermetallic compound layers at the cold and hot end was symmetrical, unaffected by thermomigration.
- The phase separation of Bi and Sn reduces the current crowding regions.

GRAPHICAL ABSTRACT

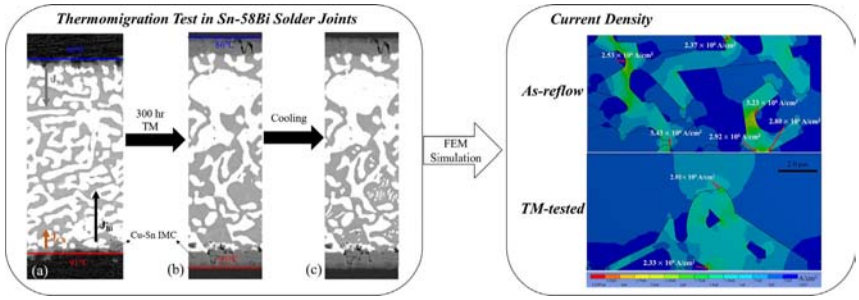

ARTICLE INFO

Article history:
Received 13 September 2018
Received in revised form 9 January 2019
Accepted 24 January 2019
Available online 25 January 2019

Keywords:
Thermomigration
Sn-Bi solder
Phase segregation
Finite element method (FEM)
Current crowding

ABSTRACT

Thermomigration (TM) has become a critical reliability issue in advanced electronic packaging because of Joule heating. A temperature gradient is required to conduct heat away, and only 1 °C of temperature difference across a 10 μm thick microbump produces a temperature gradient of 1000 °C/cm, which can cause TM, especially in low melting eutectic Sn-Bi solder interconnects. We report here that Bi atoms moving from the hot end to the cold end of the temperature gradient, are the dominant diffusing species. Under the assumption of constant volume, the Sn atoms are squeezed by the Bi atoms at the cold end and have to accommodate for the Bi atoms, which makes them move to the hot end. Consequently, the opposing fluxes of Bi and Sn are found to be about the same. Moreover, the growth of Cu-Sn intermetallic compound (IMC) layers at the cold and the hot end were symmetrical, and were unaffected by TM. Additionally, finite-element-method (FEM) simulations showed that the phase separation of Bi and Sn reduced the current crowding regions which affect the electromigration of the eutectic Sn-Bi solder interconnects.

1. Introduction

Thermomigration is atomic migration driven by temperature gradient [1–4]. As TM takes place in the Sn-rich solder joints, the Cu migration from the hot end to the cold end caused a considerable Cu-Sn intermetallic compound (IMC) growth at the cold end, which is accompanied by a serious Cu under bump metallization (UBM) consumption [5–7]. Recently, three-dimensional integrated circuit (3D IC) has become promising developments for extending Moore's Law [8]. In 3D IC, the cooling direction is going from the stacked chips with severely heat accumulation to the surface of the first-level chip (interposer) with a substantial heat-flux out by cooling design, so the

* Corresponding authors.
E-mail addresses: yashen@jwri.osaka-u.ac.jp (Y.-A. Shen), nisikawa@jwri.osaka-u.ac.jp (H. Nishikawa).

https://doi.org/10.1016/j.matdes.2019.107619

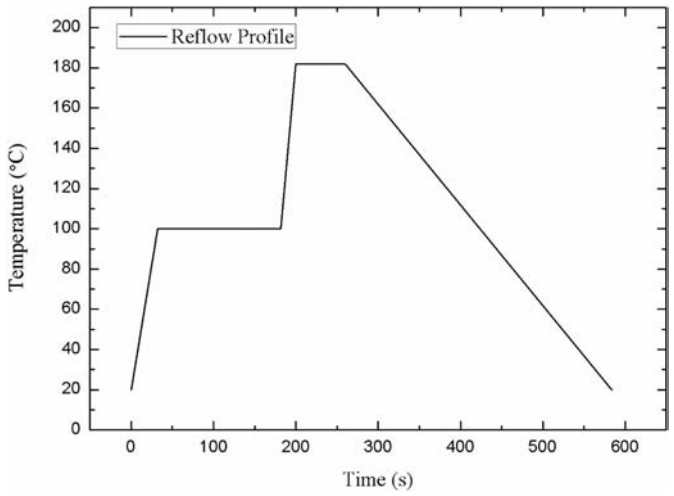

Fig. 1. Reflow profile for Cu/Sn-58Bi/Cu solder joints.

large thermal gradient with serious TM is a critical concern in solder microbumps, which connect the chips and through-silicon-vias. Moreover, with the miniaturization of solder interconnects for the continuous form-factor reduction, dimensions was downsized from flip-chip solder joints to microbumps, with the consequence of having very high temperature gradients over very low short bump heights. For example, a small temperature difference (ΔT) of 3.8 °C across a solder height of 5 μm causes a gradient of 7308 °C/cm [9]. Hence, thermomigration in microbumps is much more severe than those in flip-chip solder joints [10,11].

On the other hand, eutectic Sn-58Bi solder, which has the benefits of strong shear strength, good fatigue resistance, and good wettability on Cu substrate, has been commonly chosen as the low melting point solder [12–14]. If we consider a solder of eutectic Sn-Bi, which has a lower melting point (T_m = 138 °C) than the Sn-Ag solder (T_m = 217 °C), the TM issue is much more severe because of faster atomic diffusion. Thus, the TM reliability of low melting point solder joints is of important concern. However, the phenomenon of atomic migration caused solely by TM is hardly noticeable, not to mention the process and the details. In addition, while electromigration causes the obvious phase segregation in Sn-58Bi solders [15,16], the redistribution of the current density need to be considered because a high current density can cause serious electromigration, resulting in Cu UBM dissolution and considerable IMC formation [17,18]. Although an article shows the simulations of current densities in Sn-58Bi solders [19], the redistribution of current density caused by TM in Sn-58Bi solder microbumps are worthy of in-depth investigation.

In this study, a Cu/Sn-58Bi/Cu joint with a 42 μm solder height, bonded by a reflow process, is examined for thermomigration with a thermal gradient of 1309 °C/cm. SnBi phase segregation, a considerable Bi accumulation and Cu-Sn IMC growth at the cold and hot ends are investigated. The distributions of the current density in 6-μm Sn-58Bi microbumps are evaluated by 2-D simulations before and after being TM-tested.

The findings provide not only a much clearer understanding of the TM mechanism in Sn-58Bi solder joints, but they also shed light on issues related to the effect of TM on the electrical property of Sn-58Bi solder microbumps.

2. Experimental

A solder joint of 2-mm-Cu/42-μm-Sn-58Bi/5-mm-Cu, with a 10 mm diameter, was assembled by the reflow profile of Fig. 1. Reflow occurred in a reflow oven where the solder was melted in order to make the joint after cooling. For the study of TM, a 2-mm-Cu/42-μm-Sn-58Bi/5-mm-Cu solder joint, placed between an Al plate on a hot plate (the hot end) and an Al plate with a heat sink of a cooling fan (the cold end), was maintained at a temperature gradient of 75 to 120 °C for 300 h, as shown in Fig. 2. Two K-type thermocouples were attached on the surface of the two Cu substrates very close to the Al plates of the hot and cold end, respectively. The temperatures of the hot and cold ends were measured during the TM test, and showed a slight variation of ±2 °C because of the hot plate error. Simulation by finite element method (Ansys Workbench) was used for understanding the temperature distribution in the Sn-58Bi solder joint during the TM test. The microstructure was observed by a scanning electron microscope (SEM, JOEL-7100, Japan) with backscattered electron images (BEIs), and the phase distribution was identified by Energy dispersive X-ray spectrometer (EDS, JOEL, Japan).

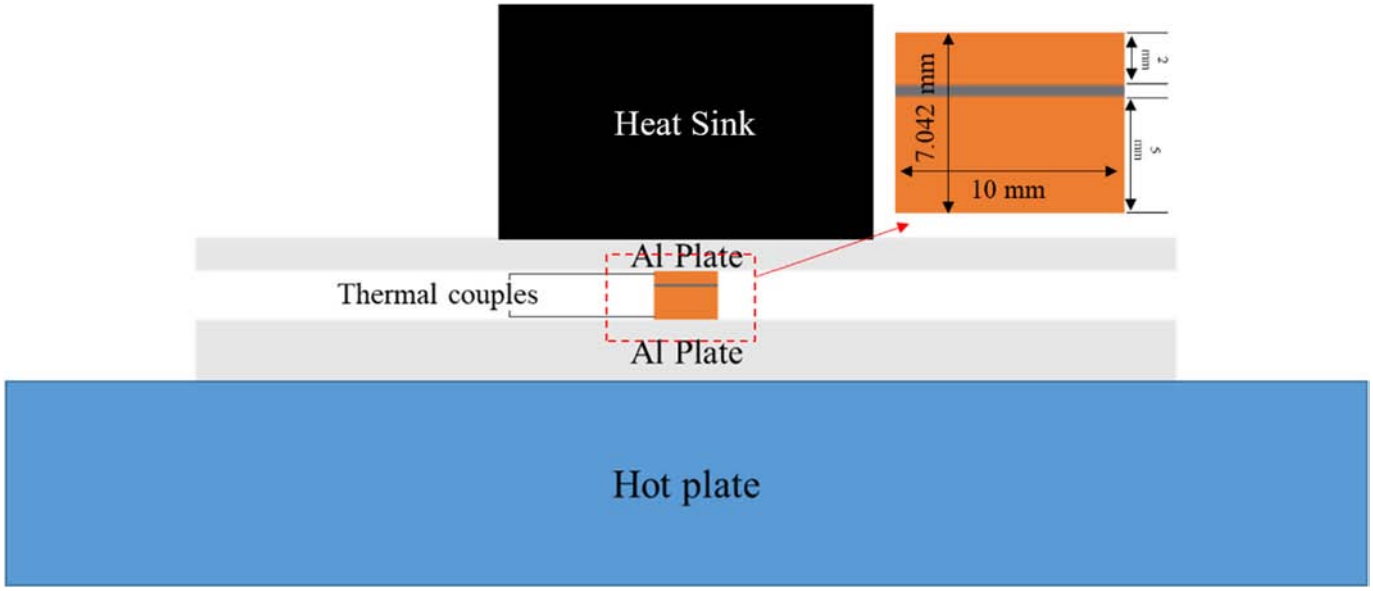

Fig. 2. Schematic diagram of TM setup and the dimension of the TM-tested solder joint.

3. Results and discussion

3.1. Thermomigration

Fig. 3 shows a three-dimensional model of 2-mm-Cu/42-μm-Sn-58Bi/5-mm-Cu solder joint, with a 10 mm diameter, for the temperature-gradient and the heat flux simulations during the TM test. In Fig. 4a, the temperature gradient is 1309.5 °C/cm, calculated by the hot-end temperature of 91.7 °C and the cold-end temperature of 86.2 °C, with 42 μm of the eutectic SnBi solder height. The average heat flux in the solder during TM is approximately 225 W/cm^2 in Fig. 4b, so the average heat transport (Q*) with 1-cm solder diameter is +176.7 J. Fig. 5a shows the SEM images of an as-reflow solder joint. The Bi and Sn phases have uniform lamellae in the solder, and most of the Bi grains have an orientation vector, directed in the transverse direction (TD). This eutectic Sn-Bi microstructure has been presented in existing literature [12]. However, after TM, we observed the significantly large Bi grains accumulated at the cold end of a Sn-58Bi solder joint, as shown in Fig. 5b. In addition, the orientation vector of the large grains is transferred from TD to the rolling direction (RD), which is parallel to the direction of the thermal gradient. Obviously, TM has affected the microstructure of the Sn-Bi solder joint. However, while the Bi accumulation at the cold end is clear, the Sn accumulation at the hot end is not obvious. This phenomenon was significant in the previous studies for electromigration in the eutectic SnBi [15], but the mechanism has not been explained for TM.

The atomic flux for TM is expressed by [4]:

$$J = C\frac{D}{kT}\frac{Q^*}{T}\left(-\frac{\partial T}{\partial X}\right) \quad (1)$$

where C is the atomic concentration, D is the interdiffusion diffusivity, and in the SnBi system, D for Bi is 4.0 × 10^{10} cm^2/s at 120 °C [20], Q* is the heat of transport, T is the temperature, k is Boltzmann constant and $\frac{\partial T}{\partial X}$ is the thermal gradient. In this TM test, in Eq. (1), we assume that $\frac{\partial T}{\partial X}$ (1309.5 °C/cm), T (361.95 K, average temperature), k (1.38 × 10^{-23} J/K) and Q* (176.7 J) are equivalent for Sn and Bi. To calculate C, we assume that the molar volume of Sn and Bi in the eutectic solder before TM is 44% to 56%. In a joint with a solder height of 42 μm and solder diameter of 10 mm, the volumes of Sn (V_{Sn}) and Bi (V_{Bi}) are 1.45 × 10^{-3} and 1.85 × 10^{-3} cm^3, respectively. The atomic mass (M_{Sn}) and density (ρ_{Sn}) of Sn are 118.7 and 7.3 g/cm^3, respectively [21], and the atomic mass (M_{Bi}) and density (ρ_{Bi}) of Bi are 209 and 9.8 g/cm^3, respectively [22]. The concentration can be expressed as:

$$C = \frac{V \times \rho}{M}\frac{1}{V}\ \text{mol/cm}^3 \quad (2)$$

The C_{Sn} and C_{Bi} are 2.7 × 10^{-2} and 2.6 × 10^{-2}, respectively. Therefore, using Eq. (1), the atomic flux of Sn (J_{Sn}) is approximately 2.77 × 10^{31} mol/cm^2 and the atomic flux of Bi (J_{Bi}) is approximately 2.69 × 10^{31} mol/cm^2 in the Sn-58Bi solder during TM. Their fluxes are roughly equal.

Moreover, in the as-reflow Sn-58Bi solder before TM, the top-half of the Sn and Bi areas are roughly equal to their bottom-half, as shown in Fig. 6. This Figure also shows that, after TM in the Bi phase, the areas near the cold end and the hot end are 57.5% and 42.5%, respectively. Specifically, before and after TM, at the hot end, the Bi/Sn areal ratio changed from about 52.7%/48.4% to about 42.5%/58.5%. Similarly, at the cold end, the Bi/Sn areal ratio changed from about 47.3%/51.6% to about 57.5%/42.5%. This clearly shows that Bi has migrated from the hot end to the cold end, following the temperature gradient. At the same time, Sn has moved from the cold end to the hot end. However, it is of interest to note that the opposing atomic fluxes of Bi and Sn are about equal. We conclude that Bi is the dominant diffusing species during TM because it follows the temperature gradient. But, the Sn flux is passive. This is because if we assume a constant volume model,

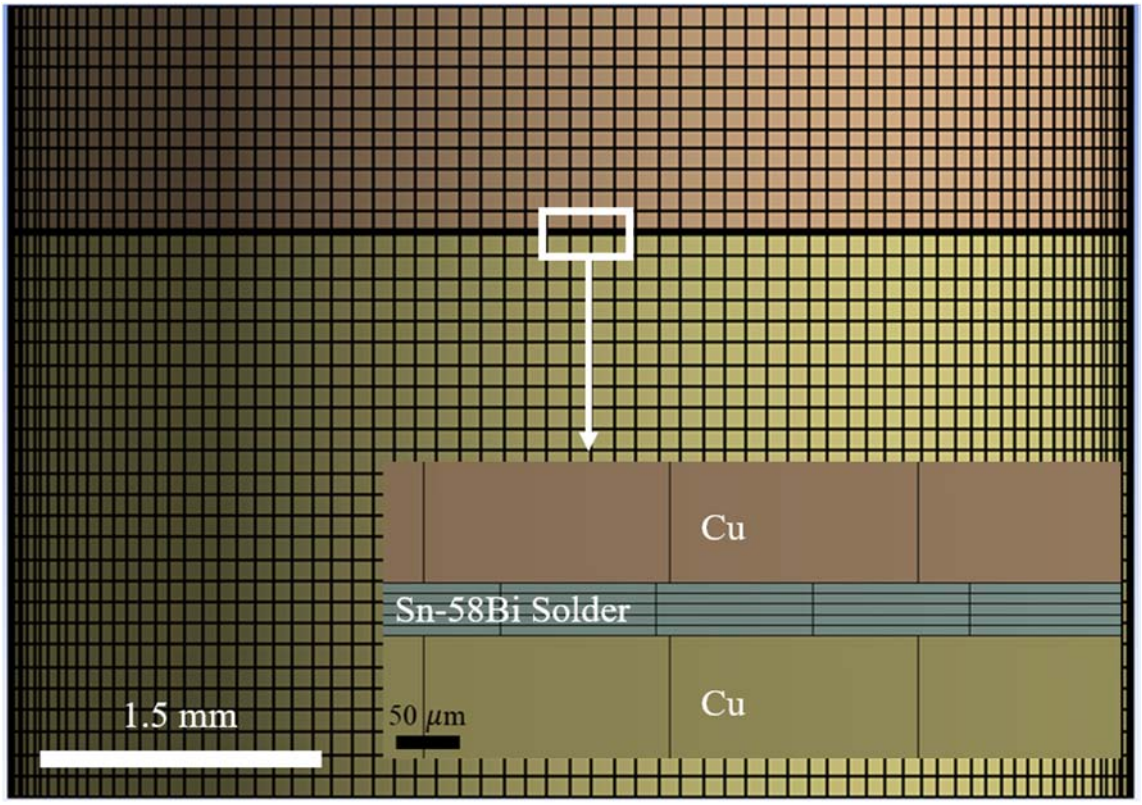

Fig. 3. The meshes in a simulation model of a Cu/Sn-58Bi/Cu solder joint.

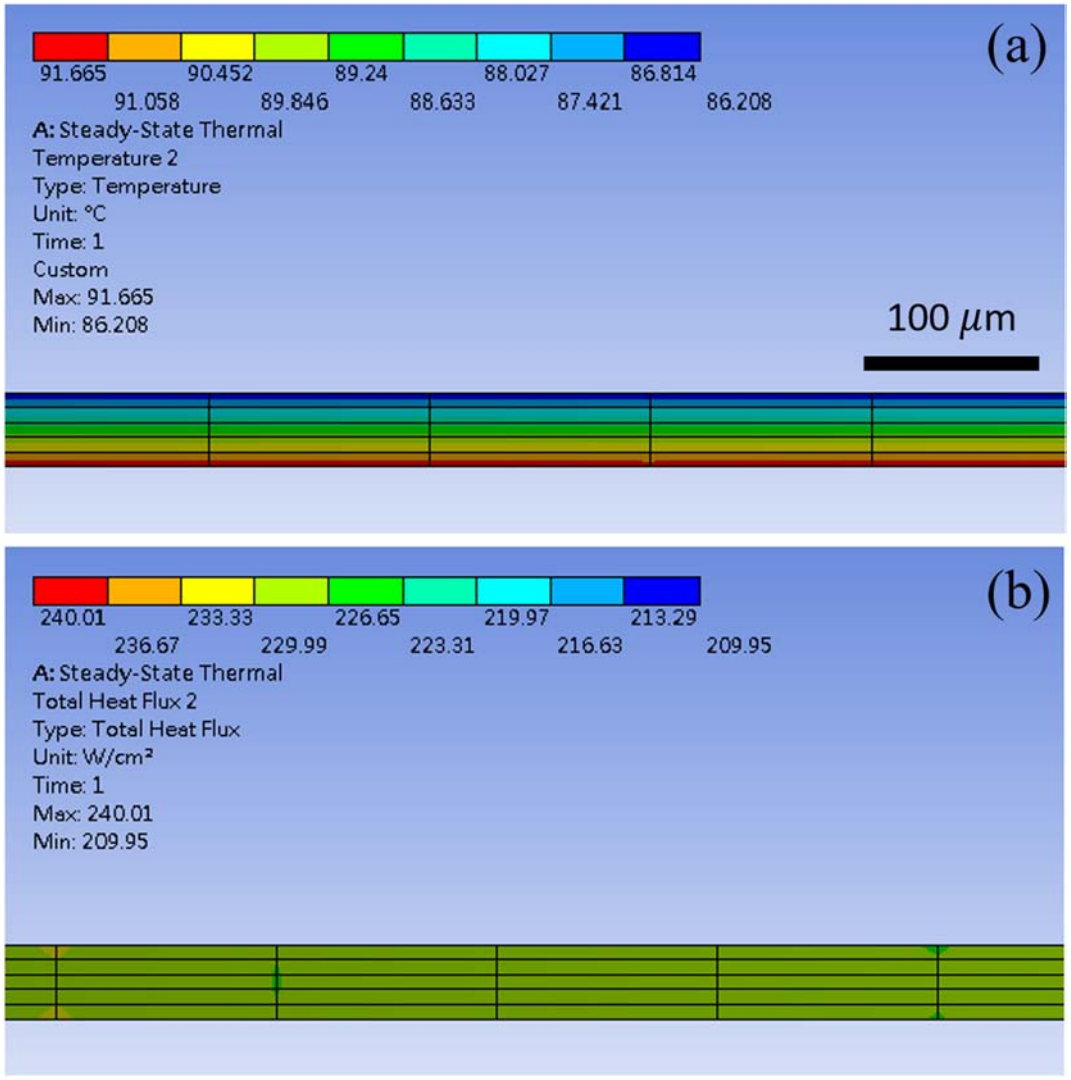

Fig. 4. The distributions of (a) the temperature and (b) the heat flux during TM in a Sn-58Bi solder joint.

the Sn atoms at the cold end will be squeezed, and they have to move away in order to make room for the arriving Bi atoms. Thus, the Sn atoms move from the cold end to the hot end. This, in turn, means that the ratio of the opposing atomic fluxes of Bi and Sn should be about equal.

3.2. Thermomigration induced microstructure changes

We investigated the changes in the microstructure, and observed that there were larger Bi grains close to the cold end but no larger Sn grains close to the hot end. Fig. 7 shows the Sn/Bi distribution in the cold-end area, the intermediate area, and the hot-end area. 42% of the Bi gathered in the cold end of the joint whereas this was only 22% for the Sn. This significantly differed from the amounts in the other two areas, where Sn and Bi were distributed evenly in both intermediate and the hot-end areas. We have concluded that the Bi is the dominant diffusing species. The migrated Bi squeezed the Sn at the cold-end site, causing Sn migration in the opposite direction. Consequently, there may not have been enough driving force for the Sn migration to reach the hot end. Additionally, at the same time, Cu-Sn IMC formation has consumed the Sn atoms in the matrix near the contact areas of the solder joint. In Fig. 8, the obviously thicker Cu-Sn IMC by about 1.5 μm at each end is evident before and after TM. Therefore, the Bi accumulation is much more significant than the Sn accumulation in the TM test. Moreover, in Fig. 5b, there are smaller Bi grains in the large Sn grains, indicated by the black frames. During the TM test, the average temperature in the solder is approximately 90 °C. From the Sn-Bi binary phase diagram, there is 10 wt% of Bi dissolved into Sn, but very little Sn dissolved into Bi. After cooling to room temperature, the Bi in Sn precipitated out and formed the smaller grains in the larger Sn grains. In contrast, the larger Bi grains were formed at the cold end site due to the 0 wt% solubility of Sn in Bi at 90 °C. The set of cross-sectional BEIs in Fig. 9a to c explains the TM process is shown. Furthermore, we consider thermomigration under a temperature gradient of 1309 °C/cm. Across an atom of diameter of 3×10^{-8} cm, the temperature difference due to the temperature gradient of 1309 °C/cm is about 4×10^{-5} K. The change of thermal energy across an atom is [23]:

$$3k\Delta T = 3 \times 1.38 \times 10^{-23}\ (\mathrm{J/K}) \times 4 \times 10^{-5}\ \mathrm{K} = 1.7 \times 10^{-27}\ \mathrm{J}.$$

If a thermal gradient induces a higher change of thermal energy than this value, thermomigration will occur too. Additionally, we prepared the other sample with a solder height of 40 μm after 300 h thermomigration between a thermal gradient of 1284.2 °C/cm, and the results are similar.

In Sn-Ag-Cu and Sn-Ag solders, the Cu UBM was substantially consumed by TM at the hot end, and abnormally thick Cu-Sn IMC were formed at the cold end [6,10]. However, in the Sn-58Bi solder,

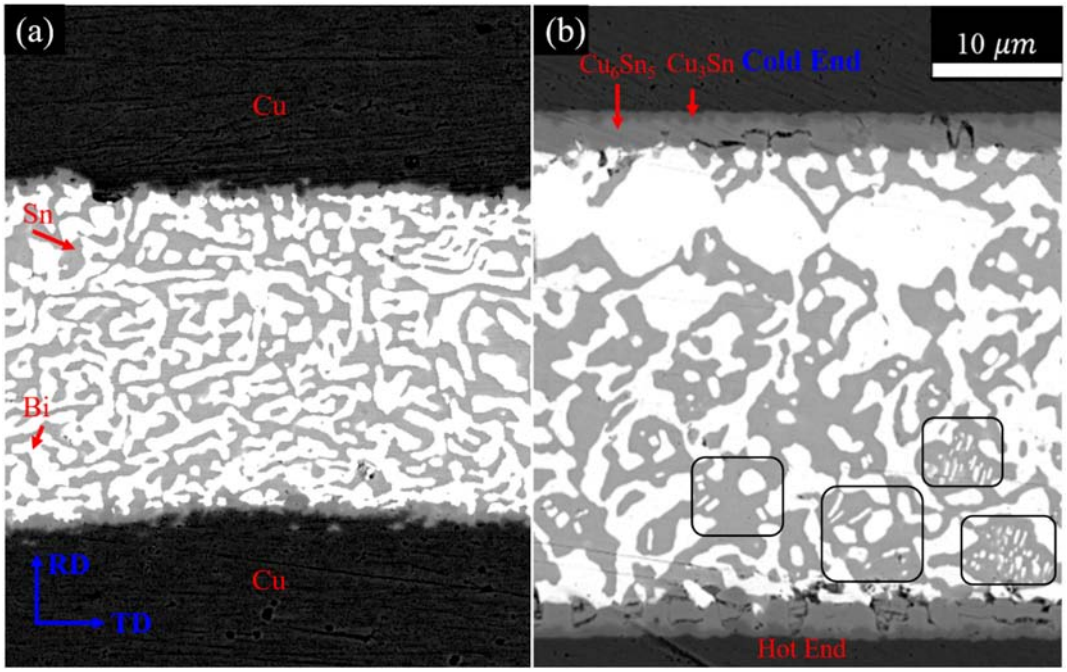

Fig. 5. The cross-section microstructures in a Sn-58Bi (a) as-reflowed before TM, and (b) after TM-tested solder joint. The bright phase is Bi and the grey phase is Sn. Precipitated grains of Bi phase in Sn are indicated by the black frames.

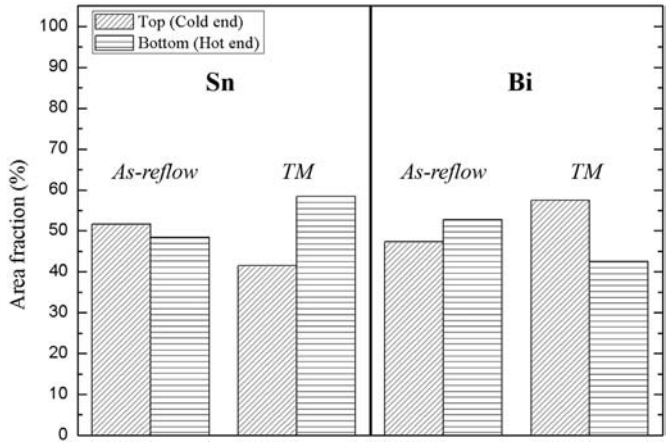

Fig. 6. Sn/Bi distribution in As-reflow and TM-tested solder joint within Top (the cold end) and Bottom half (the hot end).

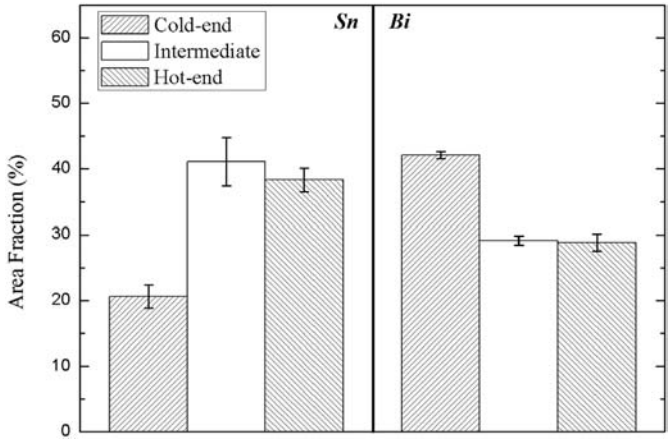

Fig. 7. Sn/Bi distribution in TM-tested solder joint within the cold-end, intermediate and hot-end area.

the Cu-Sn IMC thickness at the cold end was approximately equivalent to that at the hot end. This shows that the chemical force in forming the IMC is much stronger than the thermal force in TM in the Sn-58Bi solder joint. The constant IMC growth in the Sn-58Bi solder during TM is beneficial to the reliability of the solder joint because the UBM consumption and the considerably brittle IMC growth are avoided. Below, the effect of TM on the microstructure change and the subsequent effects on electrical properties will be examined by using FEM simulations.

3.3. FEM analysis of current-density change in Sn-58Bi solder by thermomigration

For understanding the effect of the phase segregation during TM on the change of current density in a Sn-58Bi solder, the microstructures,

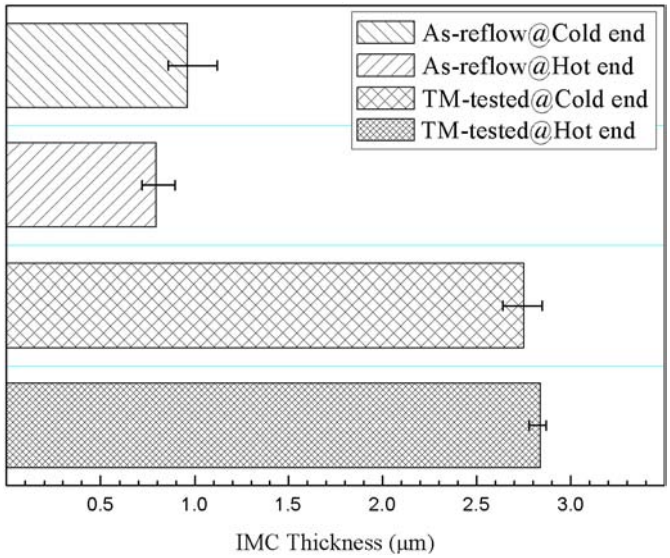

Fig. 8. Distribution of Cu-Sn IMC thickness at the cold end and hot end site.

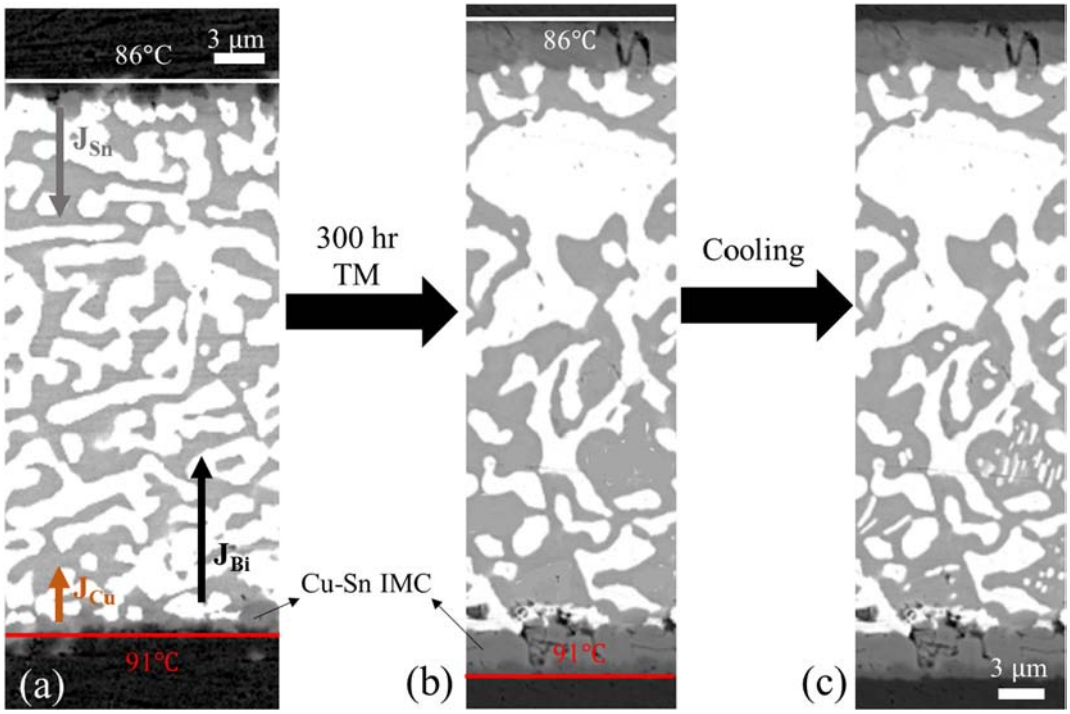

Fig. 9. Cross-section BEIs showing the microstructure evolution during TM in a Sn-58Bi solder joint. The bright color phase is Bi, moving from the hot to the cold end and the grey color phase is Sn, moving from the cold to the hot end. (b) is changed from (c) to represent the Sn-58Bi solder during TM.

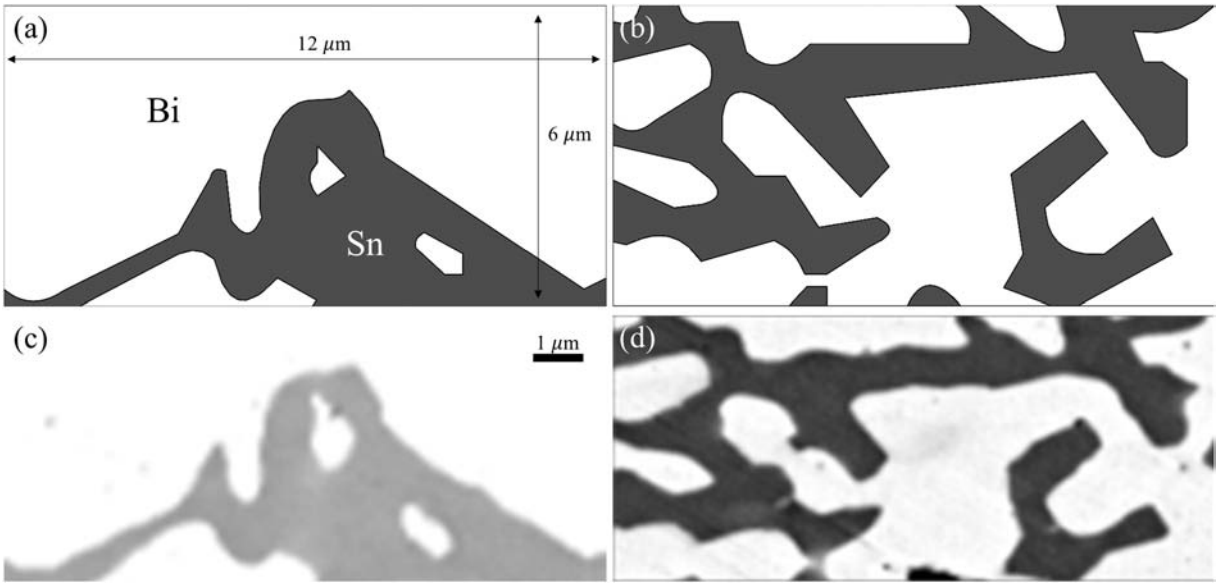

Fig. 10. The 2D model of Cu/Sn-58Bi/Cu microbumps (a) after TM test and (b) before TM test, respectively. The SEM images are the referred microstructures for the 2D model.

where with a significant phase segregation after thermomigration, are referred to create a two-dimensional (2D) model with a 6 μm × 12 μm, as shown in Fig. 10a. Fig. 10b shows an as-reflow Sn-58Bi solder, with the same dimension, which served as a benchmark. The distribution of current density in the solders was examined by an applied current of 0.056 A, which is similar to a current density of 5×10^5 A/cm^2 in a microbump with a 12-μm bump diameter. The properties of materials in the simulations are summarized in Table 1, and the boundary condition is shown in Fig. 11.

The significant redistribution of the Sn and Bi phase in the Sn-58Bi solder after TM is of urgent concern. The effect of the redistribution of Sn and Bi phase on the microstructure change is worth investigating in order to have a clearer understanding of the reliability of Sn-58Bi microbumps. Fig. 12a and b show the current density distributions in the two micro solders before and after TM, respectively. Obviously, the

Table 1
Material properties in the simulation of this study.

Materials	Electrical resistivity, μΩ·cm	Thermal conductivity, W/(m·K)
Sn-58Bi solder	–	19 [24]
Bi	129 [25]	7.97 [25]
Sn	11.5 [25]	66.8 [25]
Cu	–	401 [25]

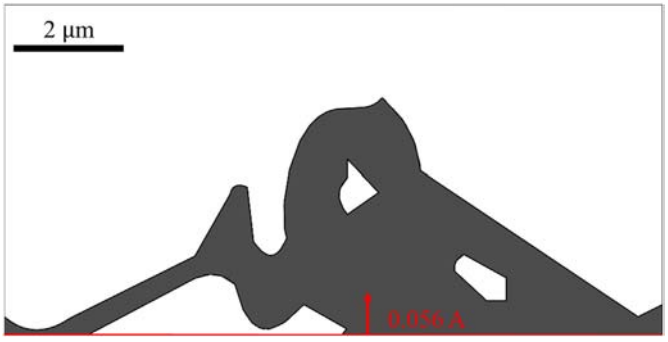

Fig. 11. Boundary condition setup for the simulations of distribution of current density.

current prefers to flow through Sn than Bi due to the much lower electrical resistivity of Sn. In the as-reflow solder of Fig. 12a, the high current-density areas with the exact values are highlighted in red arrows. Current crowding occurred in the narrow channels in Sn phase because of the uniform phase distributions of Sn and Bi. On the other hand, in the TM-tested solder in Fig. 12b, the current crowding is significantly less than that in the as-reflow solder because the Sn lamellae have become wider by TM.

The mean time to failure (MTTF) by electromigration in the interconnects can be expressed as [26]:

$$\mathrm{MTTF} = \frac{A}{j^n} e^{\left(\frac{Q}{kT}\right)} \tag{3}$$

where A is a constant, j is the current density, n is a model parameter, Q is the activation energy, k is the Boltzmann's constant and T is the absolute temperature. From the simulation results, a significantly higher degree of electromigration can be anticipated in as-reflow solders than that in TM-tested solders due to the distribution of the current density.

In this study, the eutectic Sn-Bi solder joint does not have the asymmetric Cu UBM consumption at the hot end and IMC growth at the cold end during TM. The microstructure change, which form a thicker lamellar structure, can reduce current crowding, which is very important for EM.

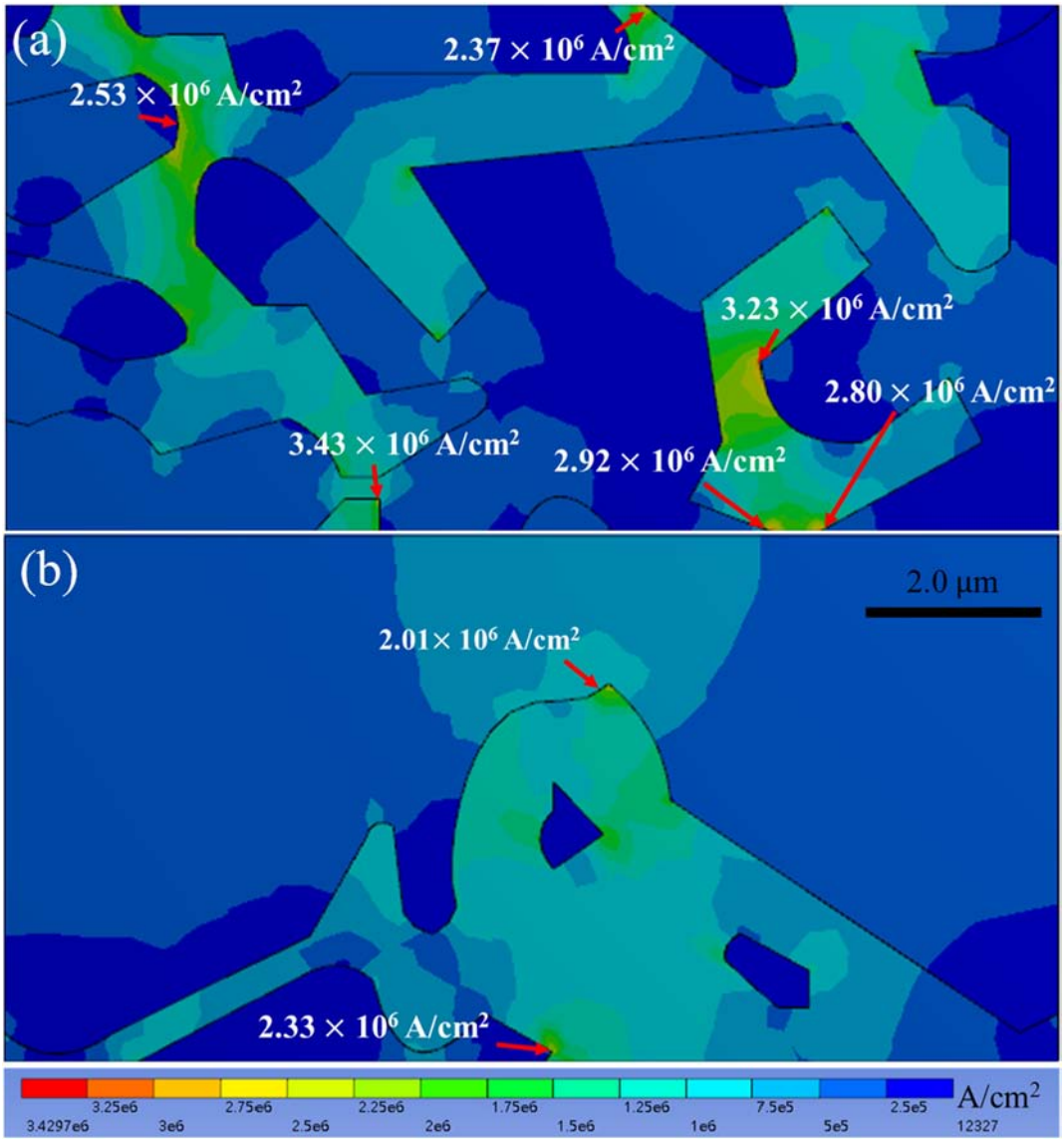

Fig. 12. Current density distributions in the (a) as-reflow and (b) TM-tested solders.

4. Conclusions

The thermomigration behavior in Cu/Sn-58Bi/Cu joint under a thermal gradient of 1309 °C/cm after 300 h is reported and analyzed. The Bi moved from the hot end to the cold end, and the Sn moved from the cold end to the hot end. The opposing fluxes of Bi (2.69×10^{31} mol/cm^2) and Sn (2.77×10^{31} mol/cm^2) were found to be about equal. However, 42% of the Bi gathered at the cold end of the joint whereas this was only 22% for the Sn. We concluded that the Bi is the dominant diffusing species. Therefore, considerable Bi accumulated at the cold end, but small Bi grains precipitated out in larger Sn grains at the hot end. And the migrated Bi squeezed the Sn at the cold-end site, causing Sn migration in the opposite direction. In addition, the change of thermal energy across an atom is 1.7×10^{-27} J. If a thermal gradient induces a higher change of thermal energy than this value, thermomigration will occur too. On the other hand, the Cu-Sn IMC growth at the hot end (from 0.9 μm to 2.75 μm) and the cold end (from 1.13 μm to 2.66 μm) were symmetrical, which shows that the Cu atoms in the Cu substrate at the hot end hardly diffused to the cold end by thermomigration. This is very different behavior from those reported for Sn-Ag-Cu and Sn-Ag solder joints in previous studies. Using FEM simulations, we showed that widening of the eutectic lamellar spacing induced by TM caused a rather uniform distribution of current density and fewer current crowding regions in a TM-tested solder. These findings indicate that the Sn-58Bi solder is a better solder with respect to UBM dissolution during TM, and its phase segregation by TM has a significant impact on reducing the current crowding regions.

CRediT authorship contribution statement

Yu-An Shen: Conceptualization, Investigation, Methodology, Formal analysis, Writing - original draft, Writing - review & editing, Visualization. **Shiqi Zhou:** Investigation, Methodology, Writing - review & editing. **Jiahui Li:** Investigation, Methodology, Writing - review & editing. **K.N. Tu:** Formal analysis, Writing - review & editing. **Hiroshi Nishikawa:** Funding acquisition, Writing - review & editing, Supervision.

Acknowledgements

The software support of Ansys Workbench from the group of N.T. Tsou in Department of Materials Science and Engineering, National Chiao Tung University, Taiwan, is acknowledged.

References

[1] D.R. Campbell, H.B. Huntington, Phys. Rev. 791 (1969) 601.
[2] H. Ye, C. Basaran, D. Hopkins, Appl. Phys. Lett. 82 (2003) 1045.
[3] C. Chen, H.M. Tong, K.N. Tu, Annu. Rev. Mater. Res. 40 (2011) 531–555.
[4] C. Chen, H.Y. Hsiao, Y.W. Chan, F.Y. Ouyang, K.N. Tu, Mater. Sci. Eng. R. Rep. 73 (2012) 85–100.
[5] W.N. Hsu, F.Y. Ouyang, Acta Mater. 81 (2014) 141–150.
[6] T.L. Yang, T. Aoki, K. Matsumoto, K. Toriyama, A. Horibe, H. Mori, Y. Orii, J.Y. Wu, C.R. Kao, Acta Mater. 113 (2016) 90–97.
[7] Y. Zhong, N. Zhao, H.T. Ma, W. Dong, M.L. Huang, J. Alloys Compd. 695 (2017) 1436–1443.
[8] K.N. Tu, Microelectron. Reliab. 51 (2011) 517–523.
[9] Y.P. Su, C.S. Wu, F.Y. Ouyang, J. Electron. Mater. 45 (2016) 30–37.
[10] Y.A. Shen, F.Y. Ouyang, C. Chen, Mater. Lett. 236 (2019) 190–193.
[11] M.L. Huang, F. Yang, N. Zhao, Mater. Des. 89 (2016) 116–120.
[12] Z. Mei, J.W. Morris Jr., J. Electron. Mater. 21 (1992) 599–607.
[13] Y. Ma, X. Li, W. Zhou, L. Yang, P. Wu, Mater. Des. 113 (2017) 264–272.
[14] S. Zhou, O. Mokhtari, M.G. Rafique, V.C. Shumugasamy, B. Mansoor, H. Nishikawa, J. Alloys Compd. 765 (2018) 1243–1252.
[15] X. Gu, Y.C. Chan, J. Electron. Mater. 37 (2008) 1721–1726.
[16] X. Gu, Y.C. Chan, J. Appl. Phys. 105 (2009) (093537-1-4).
[17] B. Chao, S.H. Chae, X. Zhang, K.H. Lu, M. Ding, J. Im, P.S. Ho, J. Appl. Phys. 100 (2006) (084909-1-10).
[18] Y.A. Shen, C. Chen, Scr. Mater. 128 (2017) 6–9.
[19] S.B. Liang, C.B. Ke, W.J. Ma, M.B. Zhou, X.P. Zhang, 66 ECTC, 2016 264–270.
[20] A.M. Delhais, D.D. Perovic, J. Electron. Mater. 47 (2018) 2057–2065.
[21] Azom, Tin, URL: https://www.azom.com/properties.aspx?ArticleID=615, Accessed date: 11 July 2018.
[22] Azom, Bismuth (Bi), URL: https://www.azom.com/article.aspx?ArticleID=9096, Accessed date: 11 July 2018.
[23] M. Li, D.W. Kim, S. Gu, D.Y. Parkinson, H. Barnard, K.N. Tu, J. Appl. Phys. 120 (2016), 075105.
[24] T. Jensen, Thermal K values list, URL: http://www.indium.com/thermal-management/thermal-k-list/, Accessed date: 11 July 2018.
[25] J.A. Dean, Table 4.1, Lange's Handbook of Chemistry, Mcraw-Hill Inc., New York 2016, p. 4.1.
[26] S.W. Liang, Y.W. Chang, C. Chen, Appl. Phys. Lett. 88 (2006) 172108.